ICSV14
Cairns • Australia
9-12 July, 2007

14th International Congress on Sound & Vibration

OPTIMISATION OF ACTIVE AND SEMI-ACTIVE NOISE AND VIBRATION CONTROL SYSTEMS

Colin H. Hansen[1], Xiaojun Qiu[2], Guillaume Barrault[1], Carl Q. Howard[1], Cornelis D. Petersen[1] and Sarabjeet Singh[1]
[1]AVC Group, School of Mechanical Engineering
University of Adelaide SA 5005 Australia
[2]The Institute of Acoustics, Nanjing University
Nanjing, China 210093
colin.hansen@adelaide.edu.au

Abstract

Active and semi-active noise control system design may be considered to be multi-variable optimisation processes. The performance of the final design is a function of the order in which various aspects of the design are optimised as well as the optimisation process chosen for each aspect. Here, the optimal hierarchy for control is discussed first of all, followed by a discussion of the optimisation of various aspects of control system design. These aspects include: the physical arrangement of reference sensors, error sensors and control actuators; the choice of cost function; the choice of control system hardware architecture; and the choice of algorithm and associated parameters. The optimisation of these variables will be illustrated with examples of work currently being undertaken by the AVC group at the University of Adelaide.

1. INTRODUCTION

The design of an effective active noise control system is essentially a multi-variable optimisation process. Variables independent of the control system include type and locations of reference sensors (for feedforward systems), error sensors and control actuators as well as the form of cost function to be minimised by the controller. Control system software variables include convergence step size, number of filter taps for control and cancellation path filters, gain settings for both error signals in and control signals out, convergence coefficient and leakage coefficient size, control filter type, cancellation path model filter type and control algorithm. Control system hardware variables include type and accuracy of the A/D converter and general control system architecture. Clearly there needs to be some sort of hierarchy in the approach to optimising the variables mentioned above. The hierarchy suggested in a previous paper [1] has been slightly modified here to reflect recent advances made in cost function alternatives and is illustrated in Figure 1. This figure indicates the order in which parameters should be optimised in order to achieve the optimal final active noise control system.

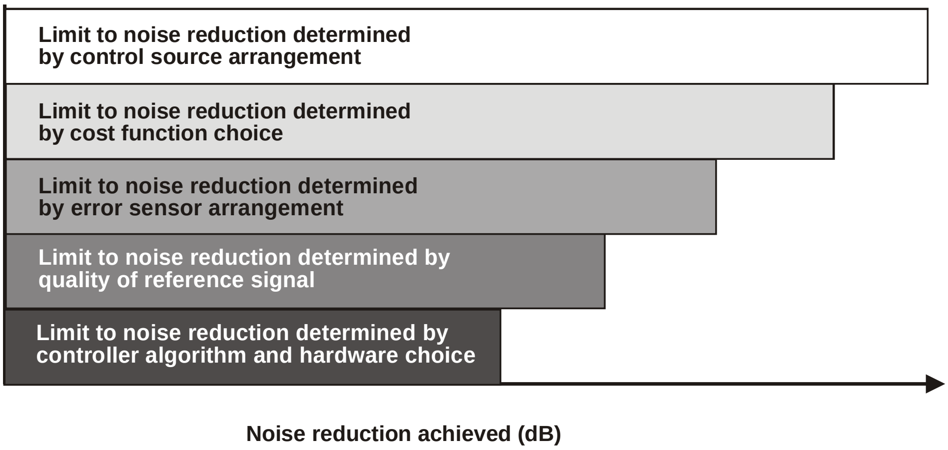

Figure 1. Active noise control system hierarchy.

The first parameter that must be optimised is the control source arrangement (number and location), as this will determine the maximum amount of cost function control achievable with an ideal error sensor arrangement and an ideal electronic controller. The control sources may be optimally arranged by using a genetic algorithm to determine the arrangement that minimises the specified cost function, which could be any one of a number of quantities including radiated sound power, global average sound pressure, energy density, pressure at one or more locations or structural vibration measures such as space averaged surface velocity.

The next parameter to be optimised is the choice of cost function that is to be minimised by the controller. This cost function is not necessarily the same as the cost function used to determine the optimum control source arrangement. For example, it may be the goal for the ANC system to minimise radiated sound power and this would be the cost function used in an analytical model and genetic algorithm to determine the optimum control source arrangement. However, it is often not possible to sense an ideal cost function such as sound power and an optimal alternative cost function has to be substituted. As another example, the cost function to be minimised may be the sound pressure at a person's ear location and this ear location may also be continually moving. In this case, it is not practical to put a microphone in the person's ear and virtual sensing may be the optimal cost function. This would allow fixed microphones to be used to minimise the sound field at a moving location. Generally, the final choice of cost function will depend on many things, including the inconvenience or otherwise of implementing the required sensors and the susceptibility of the sensors to extraneous noise that is not part of the primary noise to be controlled.

The next parameter is the error sensor arrangement (number and locations), which will determine how close it will be possible to get with an ideal controller to the maximum achievable control set by the control source arrangement. For example, if microphones are used to measure a cost function based on minimising global average sound pressure levels, it can be shown that the optimal locations for them are where there is the greatest difference between the primary sound field and the theoretically optimally controlled field. This procedure, which involves the use of multiple regression, is discussed at length by Hansen and Snyder (Ch. 8) [2].

Next is the optimisation of the reference signal, which is needed for feedforward but not feedback systems. This generally means that if the controller is to reduce sound pressure levels or radiated sound power, the reference signal should be obtained by non-acoustic means if possible (such as with a tachometer) and if a microphone is used, care must be exercised to ensure that the reference signal is not influenced by flow noise or by the control signal. These considerations are discussed in detail by Hansen and Snyder [2].

The one remaining aspect not yet considered is the optimisation of the electronic controller and this includes optimisation of the software and hardware variables discussed above. For gradient descent algorithms to be effective in optimising the control filter weights (for FIR or IIR filters) and to minimise extraneous unwanted noise being introduced into the system through the control sources, it is necessary that the reference signal be well correlated with the error signals and with the sound to be minimised.

Various feedforward and feedback ANC architectures have been discussed in many previous texts and papers [1-5] and will not be discussed further here.

The remainder of this paper will discuss in detail how each of the variables mentioned above are optimised in a practical active noise control system.

2. OPTIMISATION OF CONTROL SOURCE NUMBERS AND LOCATIONS

One of the most effective ways of optimising the number and locations of control sources to minimise a particular cost function such as radiated sound power from a structure is to use an analytical or numerical model of the system together with a genetic algorithm. An example of this approach will be provided here for the minimisation of sound transmission into a cylinder. This example will be followed by a description of the results obtained for optimisation of vibration absorbers to minimise sound transmission into the payload bay of a rocket fairing. Although this is strictly not an active control problem, the conclusions regarding the number and distribution of resonators on the fairing surface are also applicable to an active noise control system where the resonators are replaced by control actuators.

2.1 Optimisation of Control Actuator Locations to Minimise Sound Transmission into a Cylinder

The complex multi-modal nature of most practical active sound and vibration control applications involving large structures and multiple control sources, mean that an exhaustive search of all possible control source configurations is usually impractical. Even gradient-based search methods which move from point to point in the direction of maximum sound reduction (commonly referred to as a hill-climb search), are ineffective for searching for a global optimum arrangement of control source locations across many local optima. Here it will be shown that the use of a genetic algorithm can reduce the search space of a complex system to a manageable size and consistently result in an optimum control source arrangement, which provides sound reductions close to the theoretical optima. The principles underlying genetic algorithms (GAs) applied to active noise control are discussed in detail by Hansen et al. [6].

The genetic algorithm (GA) may be regarded as a guided random search that begins with the arbitrary specification of a population, typically consisting of between 40 and 100 solutions. Finding the optimal solutions involves "breeding" new solutions from the original population which involves three processes: fitness evaluation, selection of appropriate "parents" to remove (about 30%) from the population and use of the remaining parents to breed new population members ("children") for fitness evaluation using processes referred to as "crossover" and mutation, the latter being used to ensure population diversity. Fitness evaluation involves the assessment of the particular individual solution in terms of its ability to minimise the cost function in the active noise control system. For optimisation of control source locations, a particular solution is one configuration of all the control sources. The choice of parents for breeding is based on probability considerations with fitter individuals more likely to be chosen. The characteristics of the two individuals are combined randomly to produce a third individual (“child”), which becomes a member of the next generation. The breeding process continues until there are enough new individuals created to completely replace all members of the breeding population (except the fittest one when an “elitist” model is used). The breeding cycle then repeats until it is clear that further new high-fitness solutions are unlikely to be found.

The search behaviour can be altered significantly by varying the parameters controlling the algorithm such as crossover probability, mutation probability, selection probability distribution and population size. The influence that these parameters have may be described in terms of their effect on selective pressure and population diversity [7]. Selective pressure is defined as the bias that exists towards the high-fitness members of the breeding population during parent selection. Population diversity is a measure of the degree to which strings in the breeding population are distributed throughout the solution space. Selective pressure and population diversity are inversely related. For example, as selective pressure increases, the focus of the search shifts towards the high-fitness members of the breeding population, often at the expense of excluding low-fitness solutions from the breeding process. This represents a “hill-climb” procedure in which population diversity is commonly lost resulting in a narrow band of similar string types. A low selective pressure means that more members of the breeding population are included in the search process, resulting in a wider search with more diverse string combinations produced. However, in this case the search slows down due to lack of focus on the high-fitness individuals. The key to a successful global optimisation search is maintaining the correct balance between selective pressure and population diversity.

When implementing a GA, the first choice to be made is what type of coding will be used. There are two basic types, numerical (integer or floating point) and binary. Numerical integer coding implies that each possible actuator location, which could be nodes of a finite element model, is assigned a unique integer. Although maintaining a constant number of control sources is inherent to this coding method, duplicate actuator positions within individual strings are possible, requiring additional constraints to ensure that all actuator locations (in a single string) are distinct. A variation of the integer coding method is associated with the crossover process as discussed in the following paragraph. For binary coding, a binary string is used to trace the status of each possible actuator placement location in the problem space. With each possible actuator location assigned a unique position in the binary string, an actuator present is assigned a bit value of '1' in the string, with the remaining (empty) positions assigned a bit value of '0'. This scheme is not really practical for most actuator placement problems because large binary string lengths would be required to trace a relatively low number of actuators among a large number of potential actuator locations. A variation of the binary coding method is a scheme in which a multi-variable binary string (MVBS) is used to represent the positions of each actuator configuration. In this coding scheme, each individual actuator location is mapped to an n-bit binary string. To represent M actuator positions, the length of the binary string n, must satisfy the requirement: $2^n \geq M$. Once actuators are assigned a unique binary number representing their location, the binary numbers themselves are concatenated into a single (combined) binary string. To represent continuous variables in this manner, the variable range is discretised into 2^n separate equidistant values, enabling each variable value to be mapped to a distinct n-bit binary number.

Once the type of coding has been selected, a population of 40 to 100 individual strings is generated and the performance of each string in terms of minimising the cost function is evaluated. The population is then used to generate a new population using a process known as crossover. Crossover is a process where a new individual (child) string is created by the random copying of information from two parent strings, with either parent string equally likely to be the information source for each element of the child string. A biased coin toss (with a success probability, P_c) is used in determining whether the crossover will occur, or whether one parent string (with highest fitness value) is copied directly to the child population. For the example discussed here, it was found advantageous for P_c to be always set equal to one. The standard crossover method for integer coding is illustrated in Figure 2a and for binary coding in Figure 2c. It can be seen that the effect that crossover has on the variable values represented in the child string, varies significantly between coding types.

For the case of numerical strings, each position in the string (consisting of either an integer value or a discretised real number) represents the whole value of an individual search variable. When crossover occurs, the newly created child string will contain only a random mix of values that exist in either parent string (Figure 2a). This contrasts with the crossover of multi-variable binary strings, where partial exchanges of the binary information representing each search variable can occur (Figure 2c). The result of partial exchanges of binary information is that the values represented by the child string may not necessarily be the same as those in the corresponding positions of either parent (in contrast to the case of the numerical string). Thus, an inherent diversity is observed when two variable values represented as binary numbers undergo crossover.

In a traditional numerical crossover operation, the new child is generated by randomly copying string information from one or other of the parents as shown in Figure 2a. However, it can be seen that the method illustrated in Figure 2a eliminates the possibility of the two values corresponding to any particular string location for the two parents ever appearing together in the child. To overcome this problem a modified integer crossover method is used as illustrated in Figure 2b. If a duplicate is selected, it is rejected and the selection is made again. This ensures uniqueness of all actuator locations in the final solution.

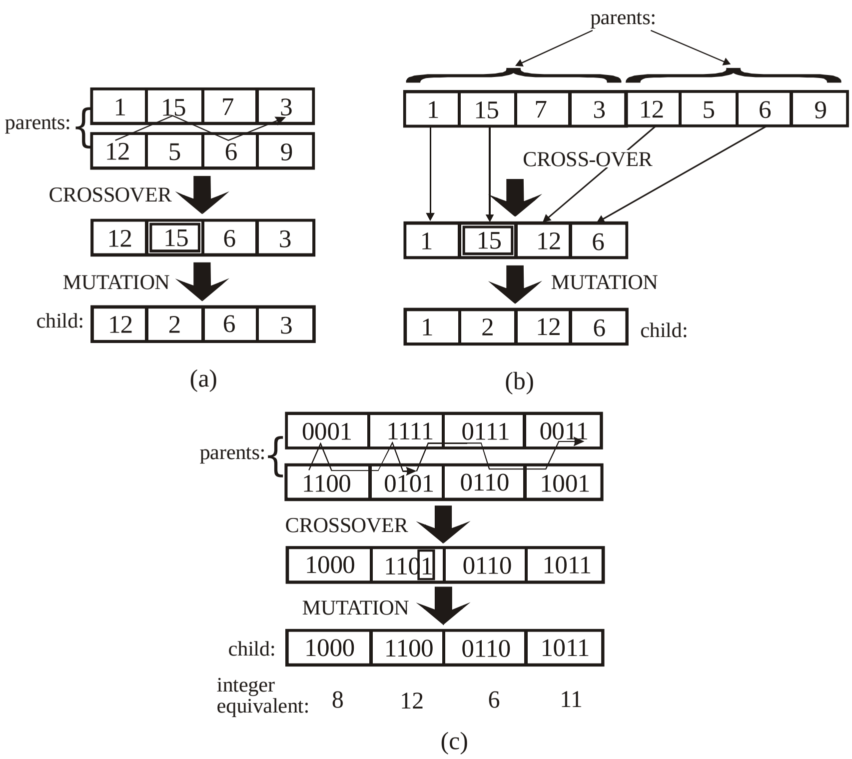

Figure 2. Illustration of cross-over and mutation for (a) normal integer coding; (b) modified integer string and (c) multi-variable binary string coding.

It is important to have a mechanism by which the population can be prevented from becoming too uniform; that is, population diversity is essential to ensure that local optima do not become the final solution. The maintenance of population diversity is achieved using a process known as mutation, where one of the string values is occasionally changed on a random basis in an attempt to prevent the irreversible loss of string information which may be vital to the progress of the search, as illustrated in Figure 2. In addition to mutation, diversity can be encouraged by penalising solutions that are similar to other solutions in the population.

Another important concept in GAs is sharing. This is a scheme that applies a penalty (based on the value returned by a summary measurement function) to the parent selection probabilities of breeding population members that are similar in the string values they contain. For the example considered here, sharing was implemented to help maintain population diversity and the details are provided in [6].

The steady state genetic algorithm (SSGA), which is discussed by Hansen et al. [6] is a variation of the standard genetic algorithm and has been developed to reduce the loss of high performing individuals from the population. The main difference with this type of algorithm is that the breeding population is sorted in order of fitness magnitude and retains the highest fitness solutions found from the entire search undertaken so far. Reproduction of new child strings (i.e. crossover and mutation) is the same as in the previous genetic algorithm (GA) case. However, after each child string is created and assigned a fitness value (by the objective function), its relative performance is immediately compared with those in the existing breeding population. If the fitness exceeds that of the lowest fitness string in the population, then the newer child string is inserted at the correct rank position in the population (displacing the low fitness solution from the bottom) and becomes an immediate active member of the breeding process. This contrasts significantly with the original genetic algorithm concept, where each child produced must wait until the next generation before it is used as a parent. Also, the SSGA eliminates the need to apply an elitist model (which explicitly retains the highest performing individual in each breeding cycle).

The GAs described above were applied to the optimisation of control actuator locations on an air-filled rib stiffened cylinder (diameter 0.9m and length 3m) with a stiffened floor and rigid end plates to minimise the transmission of 85 Hz harmonic external sound to the interior space. The cylinder, which had 30 longitudinal stiffeners attached, is illustrated in Figure 3.

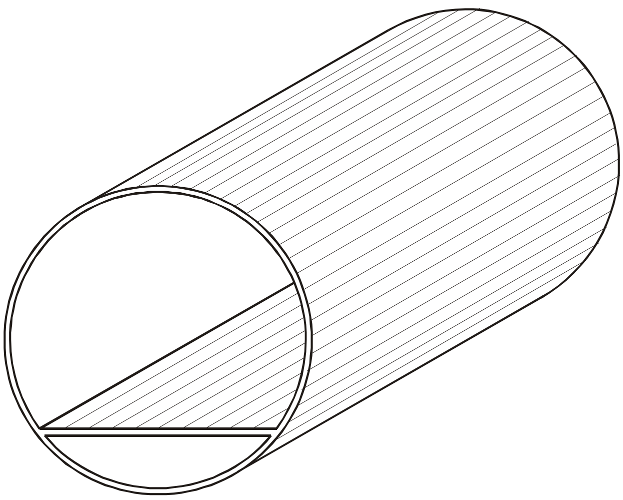

Figure 3. Cylinder model used for illustration of actuator location optimisation.

For the purposes of illustration of the effectiveness of the genetic algorithm, the external sound field was simulated using ten harmonic forces distributed randomly over the curved cylinder surface. Four control sources were available to be located on a total of 1426 locations representing a possibility of 2.89×10^9 possible actuator configurations. Details of the physical and numerical models are given in [6]. Results for each of the crossover schemes shown in Figure 2 are shown in Figure 4.

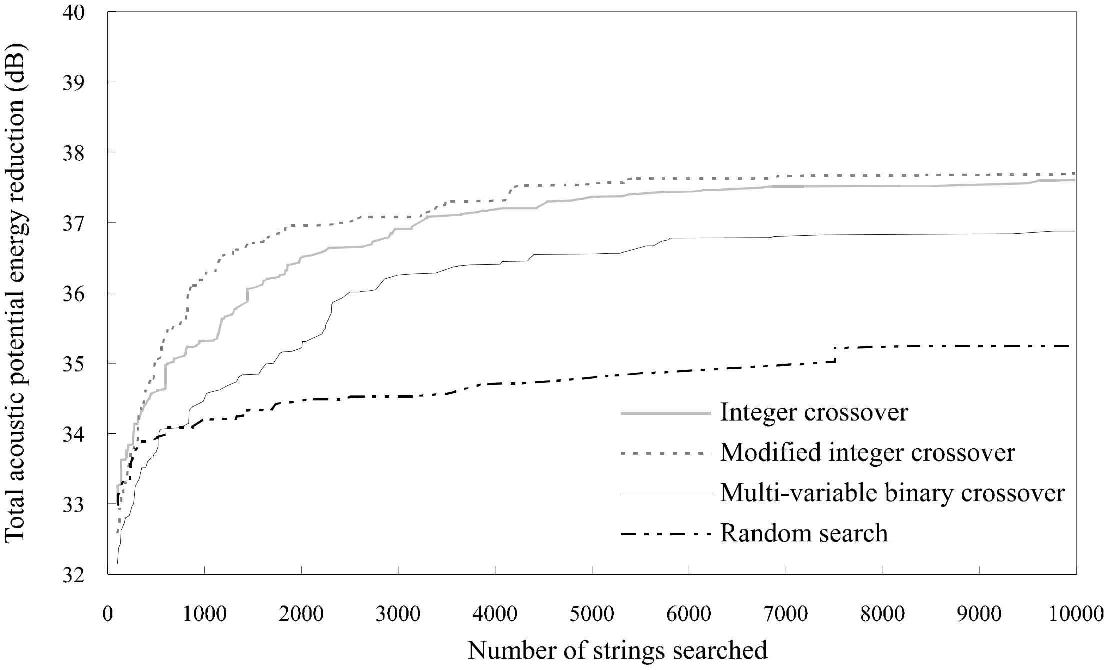

Figure 4. Best of ten search performance for the different coding schemes.

2.2 Optimisation of Resonator Configurations (Number and Locations) to Minimise Sound Transmission into a Rocket Payload Fairing

It has been commonly accepted that for active control problems, at least one actuator is required for each acoustic or vibration mode to be the controlled. Active noise and vibration control simulations and experiments to date have been conducted with a small number (less than 100) of control actuators to control a small number of modes. The results from the optimisation of a large number of passive control devices to reduce vibro-acoustic transmission indicate that there is a logarithmically diminishing benefit with the addition of more control devices. Howard et. al. [8, 9] examined the transmission loss of a rocket payload fairing when passive tuned-mass-dampers and Helmholtz resonators were attached to the fairing walls, as shown in Figure 5. It was assumed that there was a fixed added mass ‘budget’ of 10% of the total fairing mass, which meant that 6kg could be distributed amongst the control devices. Simulations were conducted using a distributed computing network and an asynchronous parallel GA to determine the optimum location and parameters of Passive Vibro-Acoustic Devices (PVADs) that would result in the minimisation of the sound levels inside a composite rocket fairing. The results from these simulations revealed several interesting outcomes, which are likely to be applicable to active control applications:

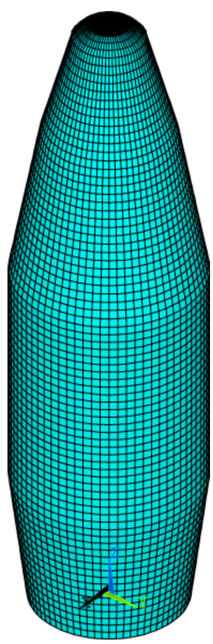

Figure 5. Rocket fairing.

- As the number of PVADs increases, the transmission loss of the system tended towards an asymptote. Figure 6 shows the Acoustic Potential Energy (APE) in the fairing, which is a measure of the average sound level. The figure shows the results from the optimisation with a varying number of PVADs attached to the fairing, again with the same amount of total added mass of 6kg divided amongst the PVADs. The figure also includes the APE of the system for the Helmholtz resonators and if the tuned-mass-dampers had been replaced with a rigid lumped mass attached at the same location as the PVAD. The comparison of these two results shows that there is indeed a benefit from having sprung masses rather than lumped masses.

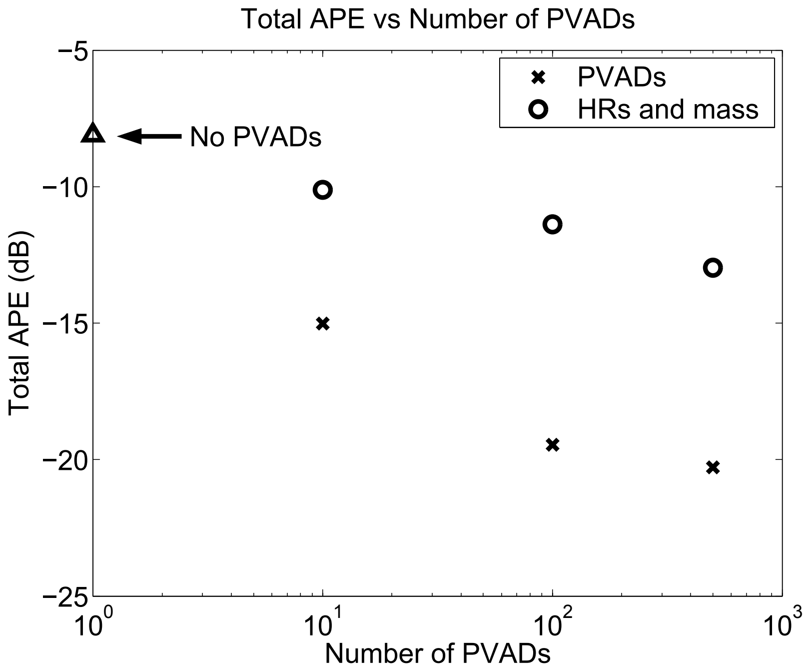

Figure 6. Acoustic potential energy in the fairing payload bay for PVADs and then with the tuned mass dampers replaced with a rigid mass.

- Each time the optimisation computations were started, the initial locations of the PVADs and their parameters were randomly selected. At the end of the optimisation, for low numbers of PVADs, the optimal locations and parameters of the absorbers were similar. For large number of PVADs there was no consistent set of ‘optimal’ locations and parameters – there were many solutions that resulted in the same value of transmission loss. This result indicates that for large number of actuators, there are numerous ‘optimal’ locations that will result in the same performance.

- Tests were also conducted to determine the sensitivity of the ‘optimal’ solutions to changes in location. Figure 7 shows two horizontal lines for the APE inside the fairing for 10 and 500 optimised PVADs attached to the fairing walls. The PVADs were then randomly re-located from their optimal locations to another location with a circle of varying radius. The results indicate that for low numbers of PVADs, the APE is sensitive to location, and for high numbers of PVADs, the APE is insensitive to location. This result indicates that for a large number of actuators, it is not important that they are placed precisely.

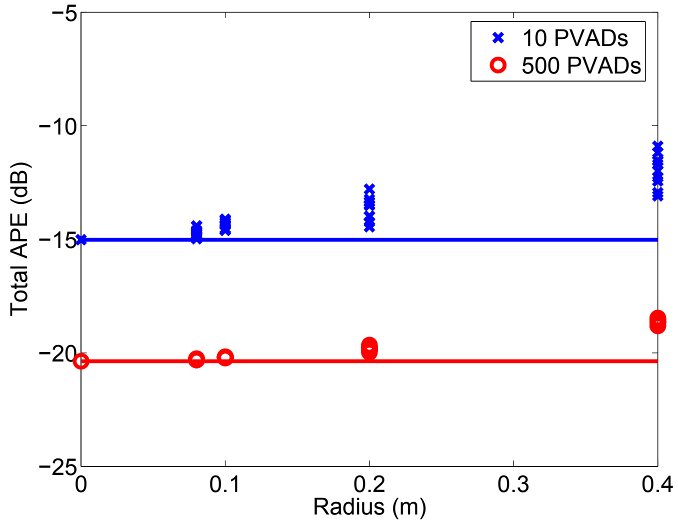

Figure 7. Acoustic potential energy in the fairing cavity for 10 and 500 PVADs randomly replaced at varying distances from their optimal locations.

3. COST FUNCTION OPTIMISATION

In many active and semi-active noise control applications, the choice of cost function plays an important role in determining the overall performance of the control system and it's important that the optimal cost function is chosen for any particular active noise control problem. In this section, two examples will be given. The first concerns the determination of the cost function that can be used by a semi-active Helmholtz resonator system to minimise the sound power transmitted along a duct system. The second concerns a solution that can be used for an ANC system to minimise noise in one or more specified locations when it is not possible to place physical error sensors in those locations. This latter solution is known as virtual sensing and will be discussed in Section 3.2. In this case, the location where the sound level to be minimised may also be non-stationary, so the virtual sensing location must move even though the physical sensors at locations remote from the virtual locations remain stationary. In some cases it may be preferable to use energy density sensing as the cost function so that there is not such a rapid change of sound level with location near the virtual sensor location.

3.1 Development of a Cost Function for an Adaptive Helmholtz Resonator for a Duct

An adaptive Helmholtz resonator is a convenient device that can be attached to the wall of a duct to minimise the transmitted sound power of a tonal noise having a wavelength that varies with time. The wavelength variation could be a result of variable source operational conditions and/or varying temperatures in the duct. Such a system is defined as semi-active as the resonator is not generating any acoustic energy itself and control of the harmonic sound propagation is achieved by changing the resonator geometry. The minimisation of sound power is achieved by the resonator generating an impedance discontinuity that reflects the energy back upstream or suppresses its generation at the source. The ideal cost function in this case would be a direct measurement of transmitted sound power. Although it is possible to directly measure the sound power associated with plane waves propagating down the duct by using two microphones mounted in the duct wall at least one wavelength downstream of the resonator, it would be more useful if it were possible to obtain a measure of the transmitted power using microphones embedded in the resonator. In the latter case, the resonator could be a completely self-contained unit.

Unfortunately it can be shown that the minimum sound power transmission condition does not correspond to a maximum or minimum sound pressure anywhere in the resonator, nor does it correspond to a maximum or minimum in the transfer function between the sound pressure in the resonator neck and the sound pressure in the resonator cavity and nor does it correspond to a fixed value of the phase of the same transfer function. It was found that the relationship between minimum sound power transmission and the phase of the transfer function between the sound pressures in the resonator neck and resonator cavity was dependent on the damping (reciprocal of the quality factor) in the resonator duct system. To find the value of the quality factor, the control system drives the piston, which forms the upper end of the resonator cavity, up and down until it finds a maximum of the ratio of the pressure in the resonator cavity (location A in Figure 8) to the pressure in the resonator neck (location B in Figure 8), as shown in [10]. The quality factor is then equal to this maximum value as shown in Figure 9. The vertical line corresponding to a cavity length of 70 mm corresponds to the minimum transmitted sound power. Once the quality factor is determined, the optimal phase difference of the transfer function may be determined by using a figure similar to Figure 10, which is for a specific family of resonators. The control system then drives the piston that changes the cavity volume until the required transfer function phase is achieved, thus minimising the transmitted power using only microphones mounted on the resonator.

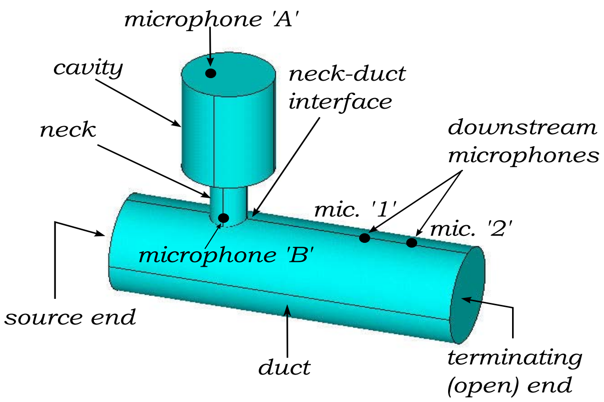

Figure 8. Helmholtz resonator set up.

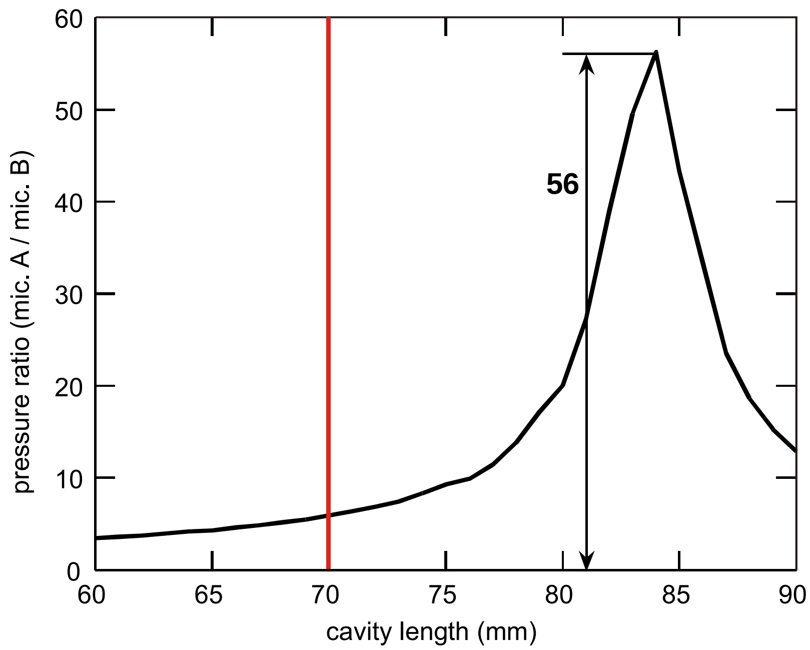

Figure 9. An example of determination of the maximum transfer function between the pressure at microphones A and B as a function of the resonator cavity length [10]. In this case the quality factor is 56.

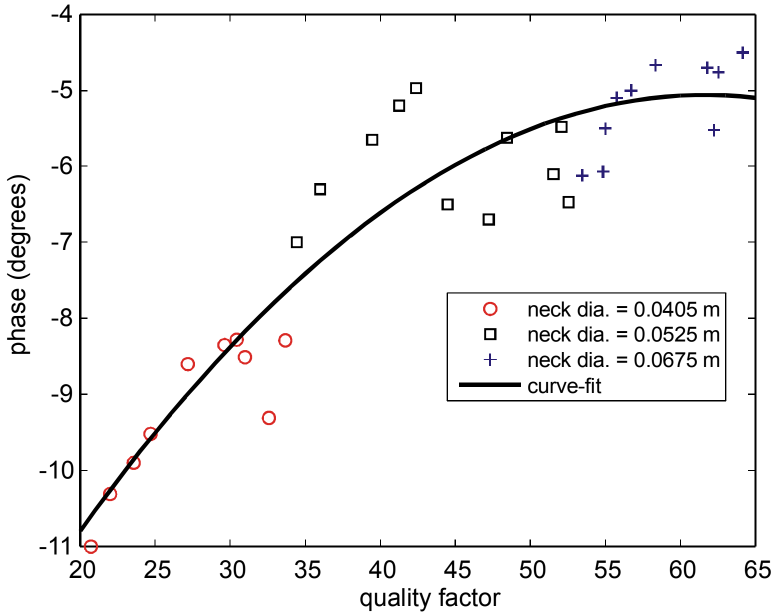

Figure 10. Transfer function optimal phase as a function of the measured quality factor of the duct/resonator system.

3.2 Optimising Virtual Sensing Cost Functions for local active noise control

3.2.1 Background

In local active noise control, the cost function that is most commonly minimised is the mean-square pressure measured by an error microphone. This generally results in a zone of quiet that is centred at the physical location of the error microphone. For a pure tone diffuse sound field, it has been shown that the size of the created local zone of quiet, in which the noise is reduced by 10dB or more, is about one-tenth of an acoustic wavelength [11]. If the observer is to experience a significant attenuation in the noise, the error microphone thus has to be located relatively close to the observer's ear, which is not always an optimal or even possible solution. This problem is illustrated in Figure 11a, where the term *physical sensor* denotes an error microphone that is physically measuring the pressure at a location in the sound field. Although a significant attenuation of the primary noise is obtained at the physical microphone

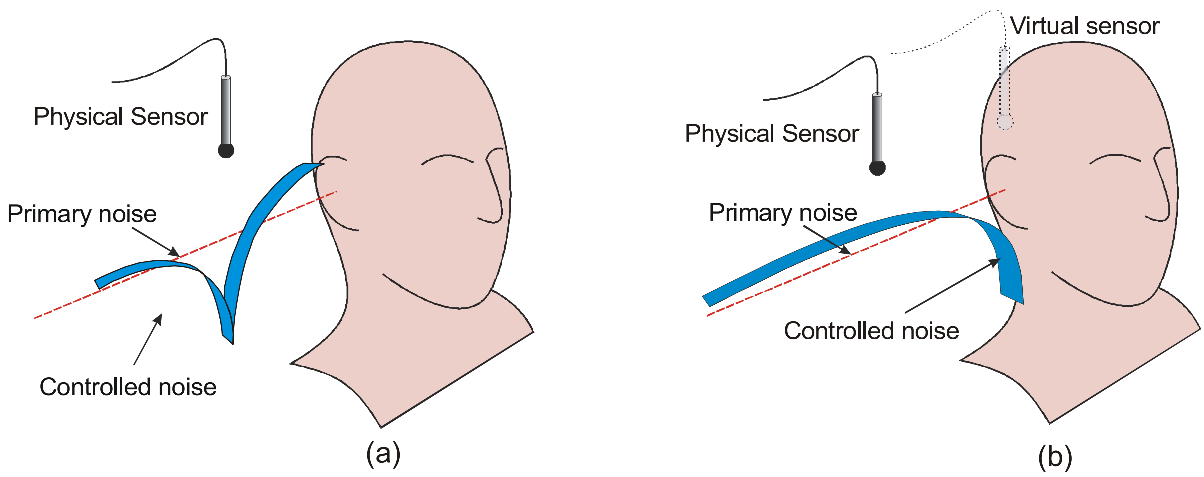

Figure 11. Local active noise control (a) at a *physical* microphone and (b) at a *virtual* microphone.

in Figure 11a, the zone of quiet is too small to extend to the observer's ear, such that the observer only experiences a small attenuation, or even amplification, in the primary noise.

To overcome the problem illustrated in Figure 11a, *virtual sensing* methods for local active noise control systems have been suggested [12-16]. The principle of these methods is illustrated in Figure 11b, where a *virtual microphone* has been located at the observer's ear where the maximum attenuation is required. Using the pressure measured by the physical microphone, the virtual sensing algorithm computes an *estimate* of the pressure at this virtual microphone. The cost function that is then minimised is the mean-square value of this estimated virtual pressure, instead of the mean-square pressure measured by the physical microphone. As illustrated in Figure 11b, this results in a zone of quiet that is moved away from the physical microphone towards the location where the maximum attenuation is required, i.e. the *virtual location*.

3.2.2 Virtual sensing algorithms

The first virtual sensing algorithm that was suggested is called the *virtual microphone arrangement* [12]. In this algorithm, models of the secondary transfer paths between the control loudspeaker and the physical and virtual microphones are estimated in a preliminary identification stage in which a physical microphone is temporarily located at the virtual location. Furthermore, it is assumed that the primary pressures at the physical and virtual microphones are equal. This assumption and the secondary transfer path models are then used to compute an estimate of the virtual pressure given the pressure measured by the physical microphone and the control signal that excites the control loudspeaker. In another virtual sensing algorithm called the *remote microphone technique* [13,14], an additional filter is used which computes an estimate of the primary pressure at the virtual microphone given the primary pressure at the physical microphone. This filter is assumed to be unity in the virtual microphone arrangement [12], and the latter algorithm is therefore a simplified version of the remote microphone technique.

In another virtual sensing method, called the *adaptive LMS virtual microphone technique* [15], an array of physical microphones is used to compute an estimate of the virtual pressure. This estimate is computed as a weighted summation of the pressures measured by the physical microphone array. The weights are determined in a preliminary identification stage in which a physical microphone is temporarily located at the virtual location. The LMS algorithm [16] is then used to adapt the weights such that the difference between the pressure measured at the virtual location and the estimate of the virtual pressure is minimised. After convergence of the weights, the physical microphone temporarily located at the virtual location is removed, such that a virtual microphone is effectively created.

A virtual sensing method based on *Kalman filtering* has been suggested as well [17]. This method uses one state-space model to describe the whole active noise control system, rather than a number of transfer path models. The pressure measured by the physical microphone is then used to compute a state-estimate given the state-space model of the active noise control system. This state-estimate is then used to compute an estimate of the virtual pressure. The state-space model of the active noise control system is estimated in a preliminary identification stage using *subspace model identification techniques* [18].

3.2.3 Number and locations of control loudspeakers, and physical and virtual microphones

When designing a local active noise control system that incorporates a virtual sensing method, the number and locations of control loudspeakers, and physical and virtual microphones have to be optimised. Since a *local* active noise control system is considered here, the number and locations of the virtual microphones are of course determined by the desired locations of maximum attenuation, which are usually the ears of an observer. The parameters that thus need to be optimised are the number and locations of the control loudspeakers and physical microphones. This optimisation can be performed in two stages.

In the *first stage*, physical microphones are initially located at the desired locations of maximum attenuation. The number of *control loudspeakers* and their locations are then optimised to ensure that the control performance that is required at the virtual locations can be obtained with the chosen control loudspeaker configuration. This optimisation can be performed as described in Section 2.

In the *second stage* of the optimisation procedure, the pressures at the virtual locations are no longer directly measured by physical microphones as in the first stage, but estimated using a virtual sensing algorithm. In the second stage, the number and locations of the *physical microphones* used by the virtual sensing are therefore optimised. To perform this optimisation, it is important to understand how the estimation accuracy of the virtual sensing algorithm influences the control performance that can be obtained at the virtual locations. It has been shown that the attenuation that can be obtained when minimising an *estimate* of the pressures at the virtual locations is always smaller than or equal to the attenuation that can be obtained when minimising the *directly measured* pressures at these locations [19], where the latter attenuation has been optimised in the first stage. The difference in the obtained control performance is determined by how *accurately* the virtual sensing algorithm can estimate the *primary pressures* at the virtual microphones given the *primary pressures* at the physical microphones [19].

In one particular virtual sensing arrangement, called the virtual microphone arrangement [12], the control performance is limited by the validity of the assumption of equal primary pressures at the physical and virtual microphones.

Other virtual sensing arrangements [14,17] do not make the assumption of equal primary pressures at the physical and virtual microphones and in these cases, there are two factors that determine the estimation accuracy of the virtual sensing algorithms. The *first* factor that determines the estimation accuracy of the virtual sensing algorithm is related to observability. If there is noise that contributes to the primary pressures at the virtual microphones, but this noise is not measured, or observed, at the physical microphones, the virtual sensing algorithm is not able to estimate this part of the primary pressures at the virtual microphones. This is related to the concept of unobservable modes of the active noise control system [20], and is thus related to the locations of the physical and virtual microphones within the sound field. Thus, the number and locations of the physical microphones should be such that all the modes that contribute to the *primary pressures* at the virtual microphones are *observable* at the physical microphones.

The *second* factor that determines the estimation accuracy of the virtual sensing algorithm is related to the issue of *causality* that often arises in active noise control problems. Causality in the context of virtual sensing can be described as follows. If there is a *causal* relationship between the primary pressures at the physical and virtual microphones, the current value of the primary pressure at the virtual microphone only depends on the current and previous values of the pressure at the physical microphone. If there is a *non-causal* relationship, the current value of the primary pressure at the virtual microphone also depends on *future* values of the pressure at the physical microphone. Thus, the virtual sensing algorithm is only able to estimate those parts of the primary pressures at the virtual microphones that are *causally* related to the primary pressures at the physical microphones. The parts that are *non-causally* related cannot be estimated and therefore reduce the estimation accuracy of the virtual sensing algorithm. Thus, the number and locations of the physical microphones should be such that these causality issues are avoided as much as possible.

3.2.4 Moving virtual microphone

The virtual sensing methods discussed in Section 3.2.2 compute an estimate of the pressure at a virtual location that is *spatially fixed* within the sound field. In a practical situation, an observer will most likely move their head, and the desired location of maximum attenuation is thus generally *moving* through the sound field rather than being spatially fixed. This problem can be overcome by using a *moving virtual microphone* that tracks the desired location of maximum attenuation. An estimate of the pressure at this moving virtual microphone can then be computed using a moving virtual sensing algorithm [21-23]. By minimising this estimate with an adaptive algorithm, a *moving zone of quiet* can be created that tracks the desired location of maximum attenuation, i.e. the *moving virtual location*. This concept has been experimentally demonstrated for narrowband noise inside an acoustic duct [21-23]. A schematic diagram of the rigidly terminated rectangular acoustic duct arrangement used in these experiments is shown in Figure 12.

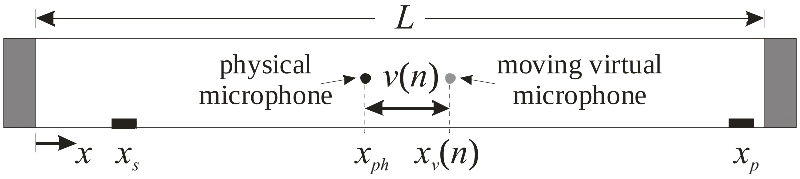

Figure 12. Schematic diagram of the rigidly terminated acoustic duct arrangement.

The acoustic duct arrangement shown in Figure 12 is of length L=4.83m, and has a primary loudspeaker located at x_p=4.73m, a control loudspeaker at x_s=0.1m, a physical microphone at x_{ph}=1.47m, and a *spatially fixed* virtual microphone at x_v=1.49m, which has not been shown in Figure 12. A *moving virtual microphone* is also located inside the duct, which tracks the desired moving location of maximum attenuation $x_v(n)= x_{ph}+v(n)$, with v the distance between the moving virtual microphone and the physical microphone, as illustrated in Figure 12. The primary loudspeaker is excited by a tonal signal of frequency 249Hz. A traversing microphone is used to measure the attenuation that is obtained at the moving virtual location $x_v(n)$. A typical result of the described experiment is shown in Figure 13.

The desired location of maximum attenuation $v(n)$ has been plotted against time in the bottom half of Figure 13. The moving virtual microphone is thus making a sinusoidal movement between a distance of 0.02m and 0.12m away from the physical microphone located at x_{ph}=1.47m, with a period of 5s. The attenuation measured at $v(n)$ with the traversing microphone has been plotted against time in the top-half of Figure 13, where the black line indicates the attenuation obtained while minimising the estimate of the pressure at the *spatially fixed* virtual microphone, and the grey line indicates the attenuation obtained while minimising the estimate of the pressure at the *moving* virtual microphone. The estimate of the pressure at the spatially fixed virtual microphone located at $v=0.02$m is computed using the virtual sensing algorithm introduced in [17]. The estimate of the pressure at the moving virtual microphone is computed using a Kalman filter based moving virtual sensing algorithm that is introduced in [23]. The minimisation of these estimates is performed using the filtered-x RLS algorithm [4] as described in [23].

The results in Figure 13 show that when the desired location of maximum attenuation $v(n)$ is moving away from the virtual microphone *spatially fixed* at $v=0.02$m, the attenuation reduces drastically from 42dB to 15dB when minimising the estimate of the pressure at this spatially fixed virtual microphone. When the estimate of the pressure at the *moving virtual microphone* is minimised, the attenuation at the desired location of the zone of quiet $v(n)$ is relatively constant over time, and does not fall below 38dB. This indicates that a moving zone of quiet that tracks the desired location of maximum attenuation has effectively been created inside the acoustic duct. The experimental results shown in Figure 13 therefore illustrate the increased control performance that can potentially be obtained in local active noise control systems when using a moving virtual sensing method instead of a spatially fixed virtual sensing method.

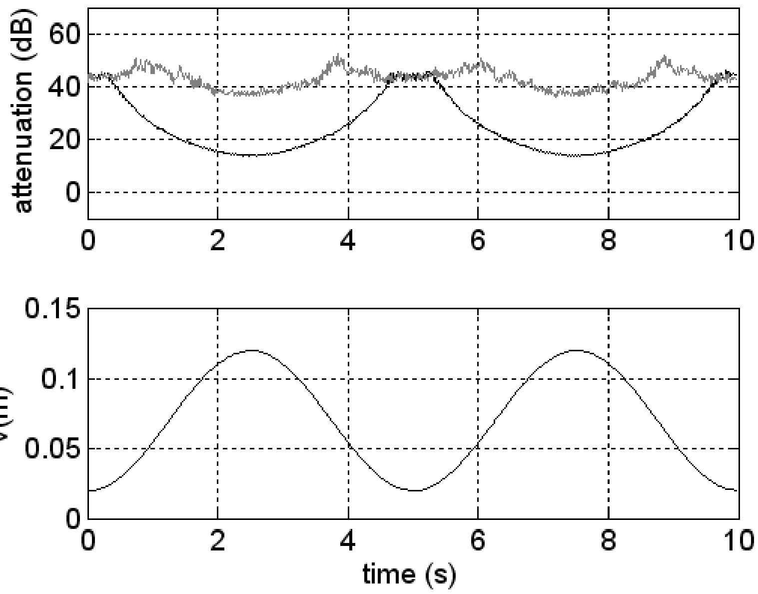

Figure 13 (*Top*) Attenuation obtained at the desired location of the zone of quiet $v(n)$ plotted against time, where the black line indicates minimising the estimate of the pressure at the *spatially fixed* virtual microphone located at $v=0.02$m, and the grey indicates minimising the estimate of the pressure at the *moving* virtual microphone that tracks $v(n)$. (*Bottom*) Desired location of the zone of quiet $v(n)$ plotted against time, with v the distance between the moving virtual microphone and the physical microphone located at x_{ph}=1.47m.

3.2.5 Increasing the zone of quiet around a virtual microphone

Instead of creating a moving virtual microphone that tracks the desired location of the zone of quiet, another approach is to try to *enlarge* the zone of quiet around a spatially fixed virtual location. This approach could for instance be used when the observer's ear is only making relatively small movements around a central spatially fixed position. In this case, the approach is thus to first move the zone of quiet away from the physical microphone to this central position, and to next enlarge the zone of quiet around this position. The enlargement of the zone of quiet can be achieved using two different approaches.

The *first* approach is to minimise estimates of the *pressure* and *pressure gradient* at the central spatially fixed virtual location, instead of only the pressure. It has been shown that the active cancellation of both pressure and pressure gradient along a single axis in a pure tone diffuse sound field using two secondary sources results in a zone of quiet that has the shape of a cylinder with rounded ends, with a length of about half an acoustic wavelength along the axis of the controlled pressure gradient, and a diameter of about one-tenth of an acoustic wavelength [24]. If only pressure is minimised, the shape of the zone of quiet is expected to be a sphere with a diameter of about one-tenth of an acoustic wavelength [11]. Minimising *estimates* of both the pressure and pressure gradient thus has the potential to increase the size of the zone of quiet created around a spatially fixed virtual location [25]. This approach is illustrated in Figure 14.

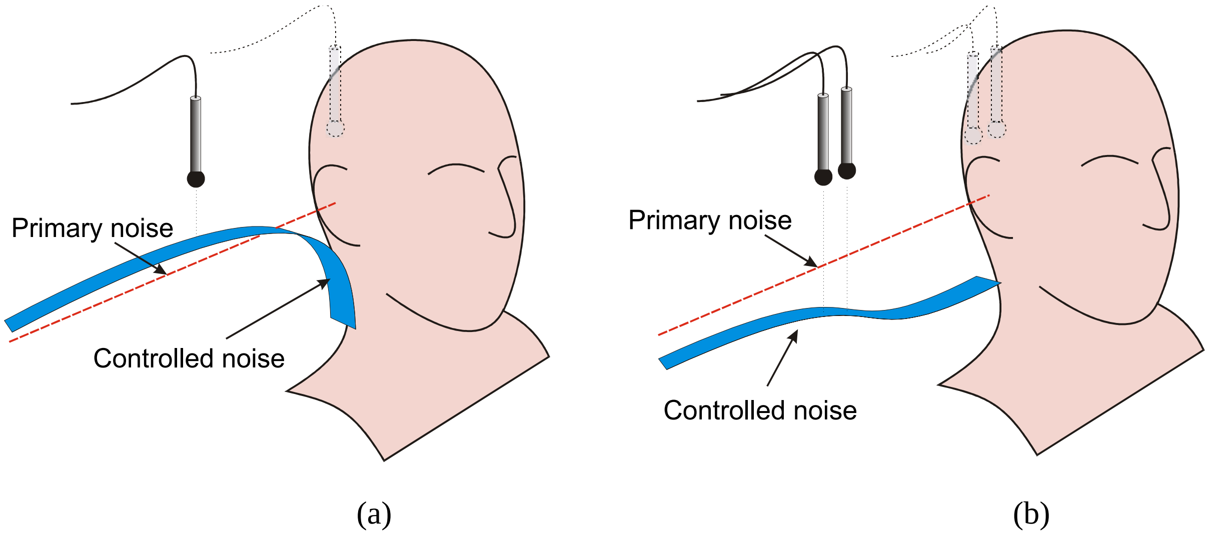

Figure 14. Illustration of the difference in pressure variation in the vicinity of a virtual sensor when energy density sensing (pressure plus pressure gradient sensing) is used instead of only pressure sensing. (a) Pressure only sensing; (b) Energy density sensing.

The *second* approach is to estimate the pressures at a number of spatially fixed virtual microphones located at and around the central spatially fixed virtual location of interest. Minimising the sum of the mean-square values of these estimated pressures is then expected to enlarge the zone of quiet around the central position. This approach has been tested in the acoustic duct arrangement shown in Figure 12, where the primary loudspeaker is now excited by broadband noise in the frequency range of 50-500Hz. The physical microphone located at x_{ph}=1.47m is used in the virtual sensing algorithm introduced in [17] to compute an estimate of the pressures at five spatially fixed virtual microphones located at v=0.04, 0.06, 0.08, 0.10 and 0.12m. In the first experiment, only the estimated pressure at the central spatially fixed virtual microphone located at v=0.08m is minimised. In the second experiment, all of the five estimated pressures are minimised simultaneously. Figure 15 shows the resulting primary and controlled sound pressure distributions inside the acoustic duct arrangement, which have been measured using the traversing microphone. The dash-dotted line indicates the primary sound pressure distribution, the grey line the controlled sound pressure distribution obtained in the first experiment, and the black line the controlled sound pressure distribution obtained in the second experiment.

The results shown in Figure 15 show that in the first experiment, the zone of quiet has effectively been moved away from the physical microphone located at v=0m towards the central spatially fixed virtual microphone located at v=0.08m. In the second experiment, the zone of quiet has effectively been moved away to the central virtual location v=0.08m as well, but is now also enlarged. However, the enlargement of the zone of quiet results in 4dB less attenuation at the central virtual location of interest. This trade-off between enlarging the zone of quiet and the reduction in the peak attenuation that is obtained at the centre of the zone of quiet is also observed when minimising the estimated pressure and pressure gradient [24].

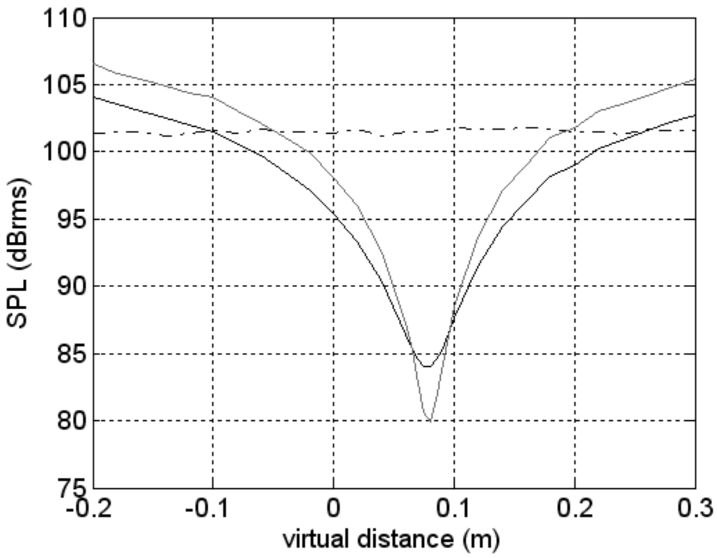

Figure 15. Moving and enlarging the zone of quiet using multiple spatially fixed virtual microphones and one physical microphone at v=0m. The dash-dotted line indicates the primary sound pressure distribution, the grey line the controlled sound pressure distribution obtained in the first experiment, and the black line the controlled sound pressure distribution obtained in the second experiment.

4. OPTIMISATION OF ERROR SENSOR NUMBERS AND LOCATIONS

Generally it is necessary to choose error sensor type, number and locations so that they provide a good measure of the cost function that is to be minimised. When radiated sound power is to be minimised, it is not usually possible to measure it directly and a measure of sound pressure has to suffice. The same applies to the minimisation of acoustic potential energy in an enclosure. If only local control is desired, then the sound pressure measurement at the location of the desired reduction seems like the optimal solution. However, it may be inconvenient to have a microphone in the exact location where maximum reduction is desired (at a person's ear for example) and this is the reason for using the virtual sensing methods described in the previous section. In addition, minimising the sound pressure at the same number of locations, as there are control sources will generate very sharp minima at the error sensor locations so that if anyone were to move their ear around the location of minimum sound pressure level, they would hear large variations in sound level as a function of location of their ear. In this case it would be prudent to use two microphones so that both pressure and pressure gradient could be minimised as discussed in the previous section and illustrated in Figure 14.

For optimal system performance, there should be more error sensors than control sources in any system unless it is only desired to minimise sound levels only exactly at the microphone locations. If it is desired to minimise a global quantity such as radiated sound power, the optimum locations of the error sensors are where there is the largest difference between the primary and optimally controlled sound fields [2] (pp. 777-780). Sommerfeldt [26] showed that this idea applies in the near field of the primary and control sources as well. For any radiating surface, the optimally controlled sound field can be determined from measurements of the primary sound field at sufficient microphone positions to provide a good measure of the radiated sound power or acoustic potential energy or any other cost function that is to be minimised. Note that each microphone output may be weighted differently before its squared value is combined with the other microphone output squared values so as to reflect its true contribution to the radiated sound power or acoustic potential energy estimate. In addition, the complex transfer functions between all control source inputs and all microphone outputs will need to be measured. With these measurements, the analysis outlined by Hansen and Snyder [2] (pp. 777-780) can be used to determine the optimally controlled sound field and hence the optimal locations for however many error sensors are to be used (usually at least one more than the number of control sources).

5. FEEDFORWARD CONTROL SYSTEM SOFTWARE OPTIMISATION

Software optimisation in a feedforward control system includes choice of algorithm as well as the optimisation of the software architecture. To begin, an example illustrating the effectiveness of choosing the correct algorithm for a particular application will be discussed and this will be followed by an illustration of how the software architecture for a feedforward control system may be optimised using multi-rate signal processing and sub-band filtering.

5.1 Software Algorithm Optimisation for Minimising Sound Radiated by an Enclosure

In the design of ANC systems to control the sound radiated externally by an enclosure excited by an interior sound source, it is usually necessary to decompose the enclosure vibration distribution into radiation modes rather than vibration modes. Each radiation mode consists of contributions from a number of vibration modes and has the property that it is orthogonal with other radiation modes in terms of sound radiation. That is, if the amplitude of vibration of a radiation mode is reduced, the sound radiated by the enclosure is guaranteed to be reduced [27, 28]. This is in contrast to vibration modes that are only orthogonal in terms of their contribution to the overall structural vibration and not sound radiation. Thus, it is generally necessary to incorporate the radiation mode model into the control system design.

In the example considered here, the enclosure is a very small and very stiff compressor housing such that the resonance frequency of the first structural mode is higher than the frequency spectrum of interest. Therefore, there are no vibration or radiation modes that can be incorporated into the control system design. In other words, the transfer function between the inside enclosure noise and the structural sensor is only a constant gain as a function of frequency. In addition, the excitation noise is periodic. This type of system is amenable to feedforward control but not feedback control as the latter is based on damping the resonant modes of the structure and there are no modes resonant in the frequency range of interest. Although it would theoretically be possible to implement feedback control by creating a model of the enclosure with virtual modes at the frequencies of interest, this approach has not yet been realised on any practical system.

As there are no radiation or vibration modes in the frequency range of interest, reducing the compressor shell vibration amplitude is guaranteed to reduce the sound radiation. Thus, it is possible to minimise sound radiation using only structural sensors and actuators only. This is an important consideration as it means that the ANC system can be completely self-contained as part of the enclosure without the need for remotely located microphones, which would be subject to problems from background noise.

Another concern in the application of ANC to industrial or consumer products is the possibility of the ANC system causing excessive inconvenience in the assembly or use of the product. In the case where the structure to be controlled is enclosed, it would not be an easy task to put a sensor or actuator inside. An internal microphone would be ideal for feedforward control, which requires a reference signal that is not greatly influenced by the control source and has a high S/N ratio. However, for the case considered here, an outside structural sensor could be just as effective, as the transfer function between the structural vibration and the inside noise is constant as a function of frequency in the frequency range of interest. Nevertheless, some compensation in the control algorithm is necessary to account for the feedback path from the control actuator to the reference sensor.

To optimise the feedforward algorithm, the feedback effects $\boldsymbol{F(n)}$ of actuators on the reference sensor have to be taken into account [5, 29, 30]. Estimates of $\boldsymbol{F(n)}$, $\hat{\boldsymbol{F}}(n)$, are modelled to account for interference with reference signals from actuator signals as shown in Figure 16.

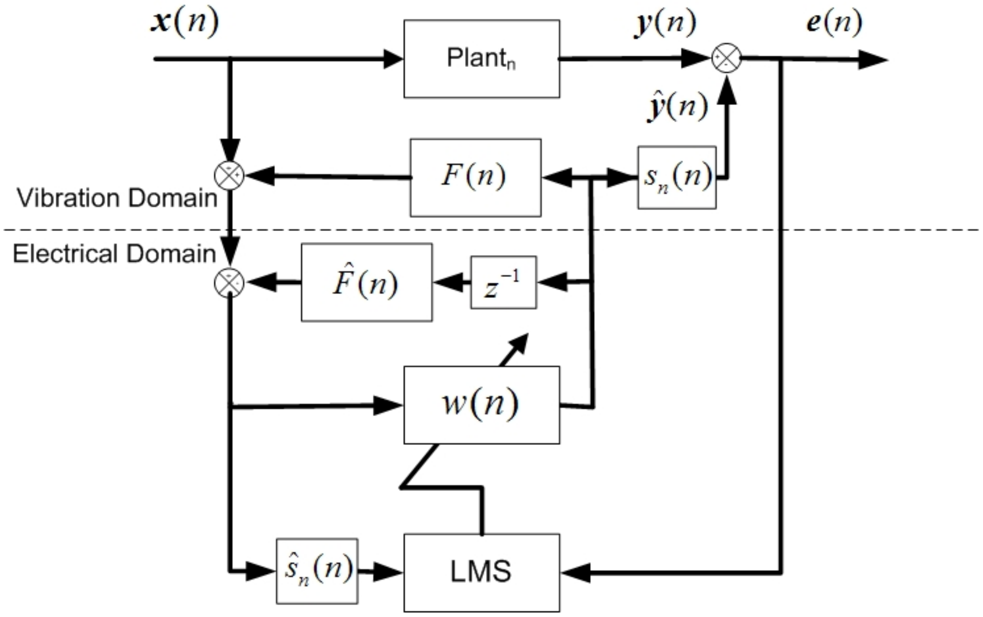

Figure 16. Detailed diagram of MIMO system showing the electronic part and the vibration/acoustic part

$\hat{\boldsymbol{F}}(n)$ are estimated simultaneously with the secondary paths $\hat{\boldsymbol{s}}_n(n)$, which are estimated off-line using a standard LMS algorithm. Plant_n are the different paths of the primary source disturbance to the sensors. The effectiveness of the noise attenuation using structural sensors/actuators is shown in [31].

5.2 Optimisation of Software Architecture using Multi-Rate Signal Processing and Sub-Band Filtering

Whenever the reference signal is available, a feedforward control system is often used due to its better control performance in terms of attenuation level and stability. To increase the upper limiting frequency and bandwidth of a feedforward control system, a higher system sampling rate often has to be used, and this brings a significant computational load, which precludes their use for many low-cost applications.

For example, consider a single channel active noise control system in a duct, where the impulse response from the control source to the error sensor is about 0.25s due to the reflections from the ends of the duct. If the noise to be controlled is below 500Hz, the sampling frequency can be as low as 1000Hz, and the length of the FIR filter for modelling the cancellation path should be about 250 taps. However, if the noise components to be controlled are up to 5000Hz, then the sampling frequency needs to be 10000Hz, and the length of the cancellation path FIR filter should be about 2500 taps. For a typical DSP processor, usually 1 instruction cycle is needed for one tap FIR filtering operation and 2 instruction cycles are needed for one tap LMS update operation; thus at least 7500 instruction cycles are needed for the control filter update of the single channel ANC system which has the FXLMS algorithm implemented. If the system needs to be updated every sample, this requires the processing capability of the DSP processor be greater than 75MFLOPS, ten times higher than that of the system with 1000Hz sampling frequency.

A number of algorithms have been proposed to reduce the computation load of the FXLMS algorithm. For example, the block FXLMS algorithm uses the sum of the mean-square errors over a period of samples as its cost function, resulting in less frequent update on block by block basis; the periodic FXLMS algorithm reduces the computational load by updating the filter coefficients every N samples with the N^{th} samples, and the periodic block algorithm is a combination of the previous two, which updates the filter coefficients every N samples with a small block of data where the block size is much smaller than that of the block FXLMS algorithm, but larger than the number of samples in a period of the disturbance. The frequency domain algorithm can also be used, which involves implementation of the control filtering in the time domain and updating of the control filter coefficients in the frequency domain.

With the above algorithms, the computation load can be substantially reduced, yet there are still some problems associated with each of them. For example, the periodic FXLMS algorithm may suffer from a long convergence time, and the implementation of the frequency domain algorithm may need large on-chip memory. There is another kind of time and frequency domain algorithm called the sub-band FXLMS algorithm, which uses multi-rate signal processing techniques. With this approach, the input signals from the reference and error sensors are sampled at a high frequency and filtered into many sub-bands. Each sub-band signal is then phase-shifted and down-sampled at a lower sampling rate and then processed to frequency shift it to a base band, which spans a frequency range from 0 Hz to an upper frequency that is dependent on the original sampling rate and the number of sub-bands used to divide up the frequency range of interest. For each sub-band, an adaptive control filter is used to provide the sub-band control signal, and the signals from each sub-band are combined and up-sampled to synthesize the full-band control signal. If each sub-band is characterised by different energy levels, then the control system performance can be optimised for maximum convergence speed in each sub-band by using a filtered-X normalised LMS (FXNLMS) algorithm where the convergence coefficient is normalised by the band signal power.

Applying multi-rate signal processing techniques in active noise control has several advantages. For example, the high sample rate sometimes can eliminate the need for sharp anti-aliasing filters and reduces the inherent one sample delay of the digital system. Each sub-band can have its own convergence coefficients and the signal dynamic range is greatly reduced in each sub-band, so the whole control system is likely to converge faster and track more quickly. However, the most important advantage is that the computation complexity for the control filter update can be greatly reduced by approximately the number of the sub-bands due to the reduced number of filter taps and weight update rate in each sub-band, and for narrow band noise, both the computation complexity and the memory requirement can be further reduced. As the sub-band FXLMS algorithm with a large number of sub-bands has more computation complexity reduction and processing flexibility in addition to the potential of a faster convergence speed, this paper will focus on the discussion of this algorithm.

The delayless sub-band adaptive architecture for the FXLMS algorithm was proposed in [32], where the signal path delay was avoided by updating the adaptive weights in sub-bands while carrying out the signal filtering in full-band with additional computation load resulting from transforming the sub-band coefficients to full-band, using the frequency stacking method. Several new schemes have been proposed to improve the performance of the sub-band-full-band weight transformation [33, 34]. Also, the sub-band cancellation path modelling and the sub-band filtered reference signal generation methods have also been proposed for the delayless sub-band adaptive architecture to further reduce the computation load [35]. The above delayless sub-band ANC algorithms were extended to multi-channel systems by Qiu et al. [36].

Sub-band filtering techniques have been widely used in the telecommunication field. However, the common sub-band structures used in adaptive echo cancellation introduce a delay in the signal path, which limits their implementation in active noise control. To eliminate the signal path delay, the adaptive weights can be updated in sub-bands while the signal filtering is carried out in full-band with additional computation load resulting from transforming the sub-band coefficients to full-band. Figure 17 shows the structure of the single channel delayless sub-band ANC system with the physical cancellation path transfer function $C(z)$, which is modelled by injecting uncorrelated random noise $r(n)$ into the system. $x(n)$ is the reference signal from the noise source and $P(z)$ is the primary path transfer function between the primary noise $p(n)$ and $x(n)$. The output of the controller $W(z)$ is $y(n)$, and the error signal $e(n)$.

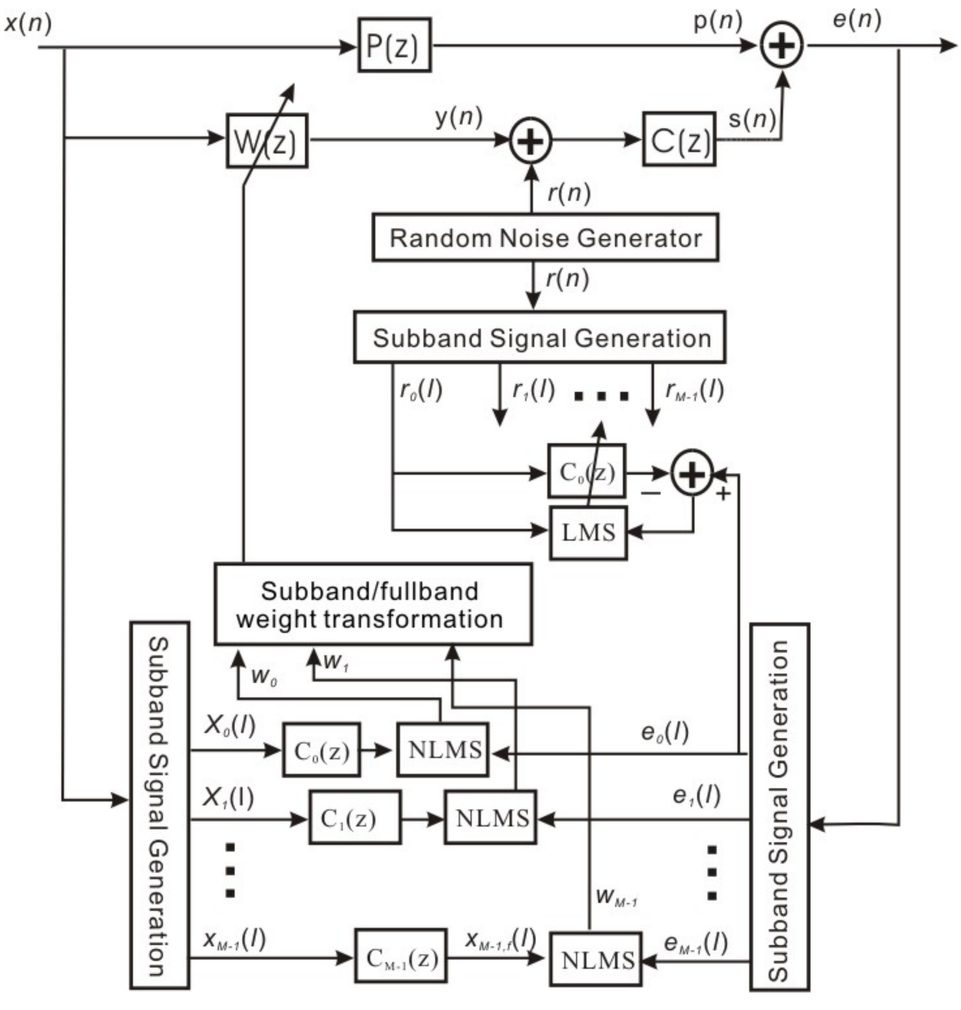

Figure 17. Delayless sub-band ANC system using the FXLMS algorithm

The system consists of 5 parts: sub-band signal generation; sub-band cancellation path modelling; sub-band adaptive weight update; sub-band/full-band weight transformation; and full-band control signal generation (control filtering). All of these are described below. The main difference between the sub-band algorithm and the common full-band FXLMS algorithm, is that, except for the control signal generation, which is carried out in full-band to avoid delay, all parts of the control system operate in each sub-band at a decimated sample rate. This reduces the computation load and allows independent and different convergence coefficients, thus allowing the controller to operate over a wider bandwidth. Note that the same sample rate is used on each sub-band, as frequency shifting is carried out on each band before down sampling so that all bands are processed in the base band. In all of the following, it is possible to replace the FXLMS algorithm with the normalised. Thus, if each sub-band is characterised by different energy levels, then the control system performance can be optimised for maximum convergence speed in each sub-band by using a filtered-X normalised LMS (FXNLMS) algorithm where the convergence coefficient is normalised by the band signal power.

As an example consider a 16kHz sampling frequency and a frequency range of interest of 0 to 4000Hz. If the sample rate is down-sampled to 250Hz for the sub-bands, then this implies that there will be 64 sub bands (16000/250). The maximum frequency for each sub-band is half the sampling frequency; that is, 125Hz. As the upper frequency of interest is 4000Hz, only the first 32 sub-bands need to be processed (4000/125 = 32), which, for a 4000Hz band-width divided into 64 sub-bands, is 0-125Hz. Note that it is possible to over sample and still have the same number of sub-bands so that many more samples are taken for each cycle. In the current example, if we wished to sample at 10 times the upper frequency of the sub-band, we still could do that and have the same number of sub-bands. This would give better results at the lower end of each sub-band.

The procedure for generating the sub-band signals will now be discussed. The m^{th} sub-band signal $x_m(l)$ is calculated by bandpass filtering, frequency shifting, and down sampling the full-band signal $x(n)$,

$$\begin{aligned} x_m(l) &= \sum_{k=0}^{K_L-1} a_k e^{-j2\pi\frac{mk}{M}} x(Dl-k) \\ &= \sum_{k=0}^{M-1} e^{-j2\pi\frac{mk}{M}} \sum_{n=0}^{K_L/M-1} a_{k+nM} x(Dl-k-nM) \end{aligned} \tag{1}$$

where l is the sub-band index, D is the down sampling frequency, a_k are the coefficients of a K_L point low pass prototype FIR filter and K_L usually is larger than the number of sub-bands M to avoid aliasing. The calculation complexity for all sub-band signal generation can be reduced by using the polyphase FFT method:

$$\left[x_0(l) \quad x_1(l) \quad \cdots \quad x_{M-1}(l)\right]^T = FFT\{\mathbf{Fx}(l)\} \tag{2}$$

where the K_L point column vector $\mathbf{x}(l) = \left[x(Dl) \quad x(Dl-1) \quad \cdots \quad x_{K-1}(Dl-K_L+1)\right]^T$, the prototype filter matrix $\mathbf{F}$ is of size $M \times K_L$, and an example with $M=4$ and $K_L=8$ is shown below.

$$\mathbf{F} = \begin{bmatrix} a_0 & 0 & 0 & 0 & a_4 & 0 & 0 & 0 \\ 0 & a_1 & 0 & 0 & 0 & a_5 & 0 & 0 \\ 0 & 0 & a_2 & 0 & 0 & 0 & a_6 & 0 \\ 0 & 0 & 0 & a_3 & 0 & 0 & 0 & a_7 \end{bmatrix} \tag{3}$$

The D new input samples are shifted into $\mathbf{x}(l)$ and multiplied with the prototype filter matrix **F**. The M sub-band signals are obtained by applying a *FFT* to the obtained M point product. In the algorithm shown in Figure 17, the reference signal, the error signal and the modelling signal are all decomposed into sub-band signals using this method. The generated sub-band signals are complex values, so complex valued adaptive filters are needed. However, as the full-band signal and the prototype filter matrix are real values, it is only necessary to do the calculation for the first $M/2+1$ sub-bands.

Figure 17 also illustrates the method used to obtain the sub-band cancellation path transfer functions where the modelling signal $r(n)$ (random noise) is decomposed into M sub-band modelling signals, which are used with the M sub-band error to directly obtain the sub-band cancellation path transfer functions. The update equation for the sub-band FXLMS algorithm in each sub-band is almost the same as that of full-band FXLMS algorithm, except that complex valued filtering and the LMS algorithm have to be used.

The purpose of the sub-band/full-band filter weight transform is to transform a set of M sub-band filter weights $\mathbf{W}_m$ of length N_s, into a corresponding full-band filter **W** of length N. Several methods have been developed, such as the DFT stacking method, the DFT-2 stacking method, the DFT-FIR weight transform and the linear weight transform. For example, by using the DFT-FIR weight transform, the full-band filter weights are obtained by using the sub-band filter weights as input sub-band signals to the synthesis filters. The full-band signal (weights) can be obtained by summation of all the sub-band signals after up sampling, bandpass filtering and frequency shifting.

It should be noted that the maximum computation complexity reduction of the single channel delayless sub-band ANC system with the FXLMS algorithm is only about 33% of that of the full-band FXLMS algorithm due to the delayless requirement. However, the computation complexity reduction provided by the multi-channel delayless sub-band ANC system with the MFXLMS (multi-channel FXLMS) algorithm can be much more. The multi-channel sub-band ANC system consists of the same 5 parts as the single channel case: cancellation path modelling; adaptive weight updating; and sub-band/full-band weight transformation. These steps are all carried out in each sub-band at the reduced sampling frequency to reduce the computation load, and only multi-channel control signals are generated by full-band FIR filters to avoid delay. Figure 18 shows the ratio of the computation complexity of the sub-band MFXLMS to the full-band MFXLMS when the sub-band number is 32, 64, 128, 256 and 512 as a function of the number of the control channels. In this case, the length of the control filter and cancellation path filter are 4096, with two times over sampling in the sub-bands ($D=M/2$). The length of the prototype filter is 4 times that of the sub-band number. It can be seen that with the increase of sub-band number, the computation load of the sub-band MFXLMS algorithm with a large number of channels can be reduced to about $8/M$ of that of the full-band. It can also be seen that when M is larger than a particular value, further increasing M cannot further reduce the computation load of the sub-band algorithm significantly, as the main contributor to the computation load becomes the control signal generation part at full-band.

6. FEEDBACK CONTROL SYSTEM SOFTWARE OPTIMISATION

There are two ways of defining the coefficients of a feedback controller. The first is known as adaptive control, and works by updating the coefficients on-line according to information obtained in real-time. In the second, an off-line modelling of the system in question must be undertaken, to enable optimal pre-defined coefficients to be determined that can then be assigned to the controller.

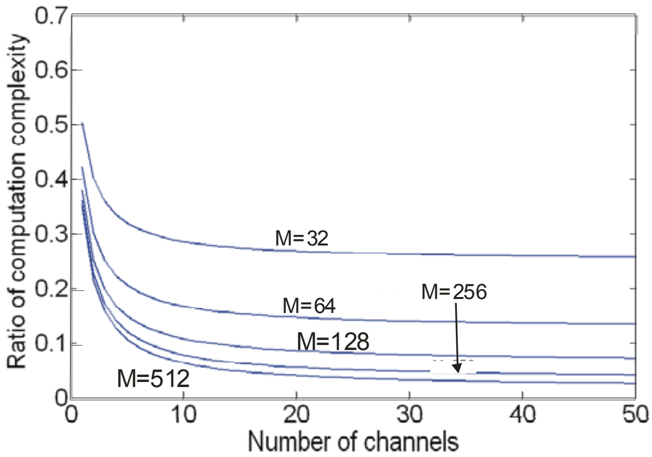

Figure 18. The ratio of the computation complexity of the sub-band to the full-band MFXLMS as a function of the number of the control channels for different numbers of sub-bands, *M*.

Existing techniques generally permit the achievement of model-based global vibration control of a given system for a specified frequency bandwidth, provided that an analytical model [37-39] or a sufficiently accurate simulation of the full system is available [40-42]. The typical complexity of real-world systems generally makes the development of analytical models virtually impossible. Even if it were possible in some cases, the time required to develop such a model would likely be excessive to the point of impracticability. There are also problems that occur with the use of simulation models, which are often grossly simplified in order to be practical. The consequence is that simulation models may be less-than-accurate representations of their actual systems, with such problems as the mismatching of resonance frequencies and damping leading to reduced controller stability and performance.

However, it is possible to derive a mathematical model of a given complex dynamic system by processing data that are obtained from the real system. This is equivalent to employing an experimental model of the system to be controlled, which is a more viable way of determining the correct dynamic features of a complex system within a specified level of uncertainty. Subspace model identification (SMI) theory [18, 43, 44], combined with spatial input/spatial output control theory [38, 45] and robust control theory [20, 46, 47] is used here to show how global vibration attenuation of a system can be ensured when a control system is derived using a mathematical model derived from experimental data of a system [48].

There are four key reasons for using a conceptual experimental model of a complex structure for the purpose of designing a global vibration controller. The first is to allow construction of a system model without requiring any knowledge of where and how the disturbance forces are applied to the system. The second is to ensure that an accurate model of the complex system is developed so the calculated vibration attenuation will be reliable. The third reason is the ability to use the resulting truncated model to control any combination of resonance frequencies that are observable and controllable by the sensors and actuators. The fourth reason is the ability to achieve global vibration attenuation of any specific part of an unknown system.

Construction of the experimental model involves using SMI theory and associated tools to extract information from data generated by the actuators and received by the sensors in the absence of any control effort. Using the SMI technique in the state-space domain allows evaluation of the matrices used in Equations (4-6) below: the system matrix $\mathbf{A}$; the actuator input matrix $\mathbf{B}_a$, with $\mathbf{N}_a$ the number of actuators; the sensor output matrix $\mathbf{C}_s$, with $\mathbf{N}_s$ the number of sensors; and the feedthrough matrix $\mathbf{D}_{sa}$ relating the actuators to the sensors.

Spatial input/spatial output control theory then enables the modelling of the system's global displacement/velocity and the contribution of the disturbances to the response of the entire structure, represented by the matrices $\mathbf{B}_f$ and $\mathbf{C}_y$ in Equations (4-6). Given that the SMI technique provides a state-space representation of the system up to a similarity transformation, the final step in the process of building an experimental model is to use a similarity transformation to transform the matrices $\mathbf{A}$, $\mathbf{B}_a$, $\mathbf{D}_{sa}$ and $\mathbf{C}_s$ to the same orthogonal subspace as $\mathbf{B}_f$ and $\mathbf{C}_y$. The equation system for representing the system in question can be written as:

$$\dot{\boldsymbol{x}}(s) = \mathbf{A}\boldsymbol{x}(s) + \mathbf{B}_f \boldsymbol{f}(s) + \mathbf{B}_a \boldsymbol{v}_a(s) \tag{4}$$

$$\boldsymbol{y}(s) = \mathbf{C}_y \boldsymbol{x}(s) \tag{5}$$

$$\boldsymbol{v}_s(s) = \mathbf{C}_s \boldsymbol{x}(s) + \mathbf{D}_{sa} \boldsymbol{v}_a(s) \tag{6}$$

where $\boldsymbol{x}$ is the state of the system, $\boldsymbol{f}$ is the disturbance, $\boldsymbol{y}$ represents the displacement output at a particular location, $\boldsymbol{v}_s$ represents the sensor outputs, and $\boldsymbol{v}_a$ represents the actuator inputs.

Because the model must be truncated for practical reasons, the performance of the controller is directly determined by the reduced model $\mathbf{G}_r$(s), and the way in which it is reduced. To maintain high controller performance, the model must take into account the residual system dynamics $\mathbf{G}_d$(s), due to excitation of higher frequency modes. This has been done by others [49] who show the required relocation of poles and zeros to account for the model truncation. However, in the analysis [49], all the lower modes are included in the model. As previously mentioned, when the focus is only on a specified frequency bandwidth, maximising the control efficiency in the bandwidth of interest requires the truncation of the modes above and below that bandwidth. In this case, to account for the altered poles and zeros as a result of the truncation, it is necessary to account for the lower order modes using a low frequency residual dynamic $\mathbf{G}_l$(s), as well as for the higher modes using a high frequency residual dynamic $\mathbf{G}_d$(s). This problem can be addressed using the convex optimisation proposed by Barrault et al. [50].

With Figure 19, the idea is to evaluate the optimal feedthrough term $\mathbf{K}_d$ and second-order term $\mathbf{K}_l$ of the truncated transfer function, $\hat{\mathbf{G}}(s) = \mathbf{K}_l/s^2 + \mathbf{G}_r(s) + \mathbf{K}_d$, of the full experimental model, $\mathbf{G}(s) = \mathbf{G}_l(s) + \mathbf{G}_r(s) + \mathbf{G}_d(s)$, by minimising the $\mathcal{H}_2$ norm of the following cost function J:

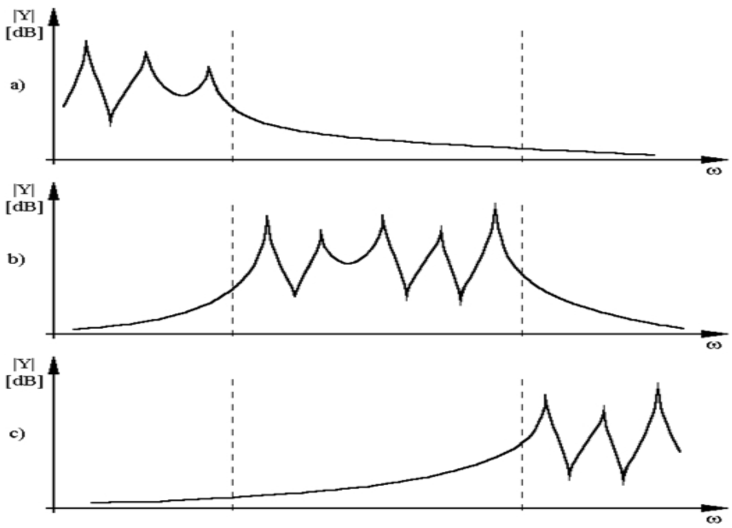

Figure 19. Mode contributions to energy inside and outside the frequency bandwidth of interest: a) low frequencies, b) frequencies of interest and c) high frequencies.

$$J = \left\| W\left(\boldsymbol{G}(s) - \widehat{\boldsymbol{G}}(s)\right)\right\|_2^2 \tag{7}$$

where W is a band-pass filter that has a unit value in $[\omega_a, \omega_c]$ with $\omega_c = (\omega_{m2} + \omega_{m2+1})/2$, $\omega_a = (\omega_{m1} + \omega_{m1-1})/2$ and *m1* is the mode number of the first vibration mode of interest, *m2* is that of the last one.

As an example, the full experimental model **G**(s) of a cantilever beam is compared with three truncated models: one without any correction terms $\mathbf{G}_r(s)$, one with only the zeroth order term of $\mathbf{K}_d$, and one with both terms $\mathbf{K}_l$ and $\mathbf{K}_d$. Figure 20 shows the effect of the correction terms. The bandwidth of interest is from 100Hz up to 900Hz.

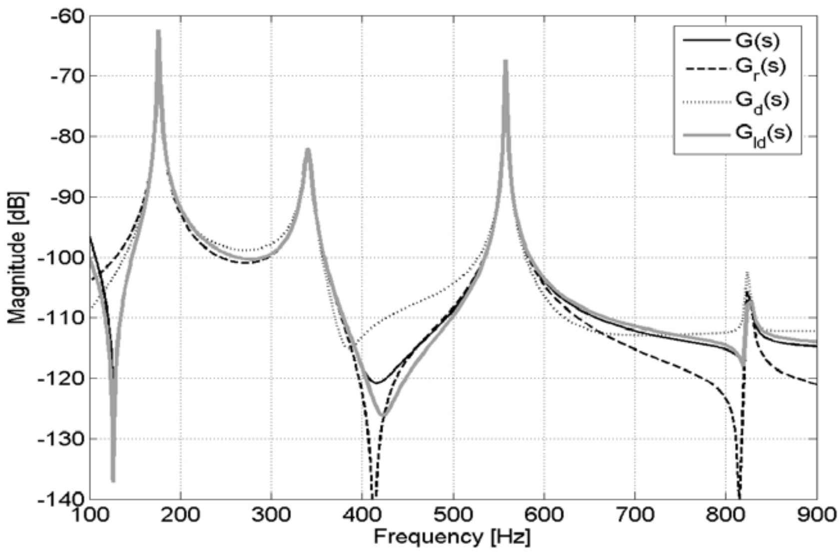

Figure 20. Frequency response v_s/v_a due to model truncation and corrections. G(s) = the full experimental model, $G_r(s)$ = the truncated model without any correction term, $G_d(s)$ = the truncated model with the optimal zero-order term of K_d and $G_{ld}(s)$ = the truncated model with both optimal terms K_l and K_d.

7. CONTROL SYSTEM HARDWARE OPTIMISATION

There are currently four possible paths that may be followed in the hardware development for a new active noise controller. These are: (1) use currently available commercial general purpose DSP systems that can be programmed for ANC in a high level language such as C; (2) use a standard input/output board embedded in a PC and an operating system dedicated to real time processing; (3) use a general-purpose DSP board in a custom enclosure with power supply and custom I/O boards (4) develop a multi-processor DSP board from scratch with sufficient power and memory to meet the most demanding ANC application. Include it in a modular system that allows the use of multiple DSP boards and multiple IO modules, which can be tailored to the number of channels needed and the processing power and memory required.

Although the fourth option offers more flexibility in terms of producing a system optimised for active noise and vibration control, it needs considerably more effort and financial resources. Generally, options (1) and (2) above are usually suitable only for laboratory demonstrations. Option (3) could potentially be used to develop commercial systems, but the available general purpose DSP boards are difficult to use and interfacing them with other hardware usually results in numerous problems. In addition they are usually based on out of date DSP chips. Option (4) above is the best approach as the most up to date DSP chips can be used and the hardware can be optimised for ANC applications, provided that there are sufficient time and financial resources available. As option (3) is the least useful, it will not be discussed further here. The most well known system that may be classified as option (1) is d-Space, provided by the MathWorks company. This system is used by many researchers and will not be discussed further here.

Option (2) uses a standard Input/output card in a PC and an Operational System (OS) and Freeware (QNX or Linux) dedicated to real-time processing. It can be installed on any general-purpose computer. The advantage of this approach is that it allows the design of embedded systems for direct application of the type FPGA (Field Programmable Gate Array), without requiring the designer to have knowledge of machine language (VHDL). This technology is currently rarely used because it is still new, but the interest from industry has been growing considerably in the past several years as its viability increases with dropping costs. The most well-known software engines are XPCTarget and RT-LAB provided by MathWorks and Opal-rt respectively. The intention of these software packages is to overcome the restrictions of real-time operation using other software that is already well developed from the theoretical point of view in the areas of mathematical calculations, signal processing and automation. One of the original aspects of RT-LAB is the use of a cross-platform, open-source scripting language called Python, whose use is growing in popularity, particularly for technical applications. Its syntax is very close to m-script, which has become very popular among Matlab users. It is object-oriented and allows users to automate applications on any platform. The RT-LAB API allows users to configure models and automate test runs using the Python language. Also, because Python is multi-threaded, it is possible to interface to multiple concurrent models, running on several target processors. This means that it is possible to program several different tests, and even have data flowing from one test platform to another from a single operator station. In other words, this functionality allows the generation of a statistical representation of experiment or process behaviour, which is a valuable laboratory tool.

An example of a system that satisfies Option (4) above is illustrated in Figure 21, which shows the architecture of the third generation controller, EZ-ANC III, which is being developed in the University of Adelaide. Each I/O module contains simple signal conditioning hardware such as a two order low pass filter, a short delay A/D and D/A converter sampling at a high frequency and a low cost DSP, which provides ample processing power for the I/O management tasks and multi-rate signal processing as well as transducer failure and signal overload management. The adaptive signal processing and system modelling are carried out in the central processor module, which contains an array or a cluster of DSPs with a huge amount of shared global memory and an interface for a PC.

The sub-band MFXLMS algorithm is especially suited to the EZ-ANC III mentioned above. For example, assume that a 16 channel ANC system with a 16 kHz sampling frequency is used to reduce noise below 4000 Hz. The number of sub-bands is 128, which makes the control filter update rate decrease 64 times if the over sampling rate is two times. This is equivalent to an ANC system with a sampling rate of 250Hz. The low cost DSP used in each I/O module is the ADSP-21369, which is a third generation Analog Devices SHARC® Processor running at 400MHz with 2Mbits on-chip SRAM and 6M bit of on-chip mask programmable ROM. The sub-band signal decomposition, sub-band to full-band weight synthesis, real time full-band control filtering at the 16 kHz sampling rate and other management tasks can be implemented on this local processor with the related code burned into the ROM. The 16 channel control filter update, 256 channel cancellation path modelling and 256 filtered reference signals generation are carried out in the central processor module, which also contains an ADSP-21369 processor with more than 512M shared global memory and an Ethernet interface with the PC.

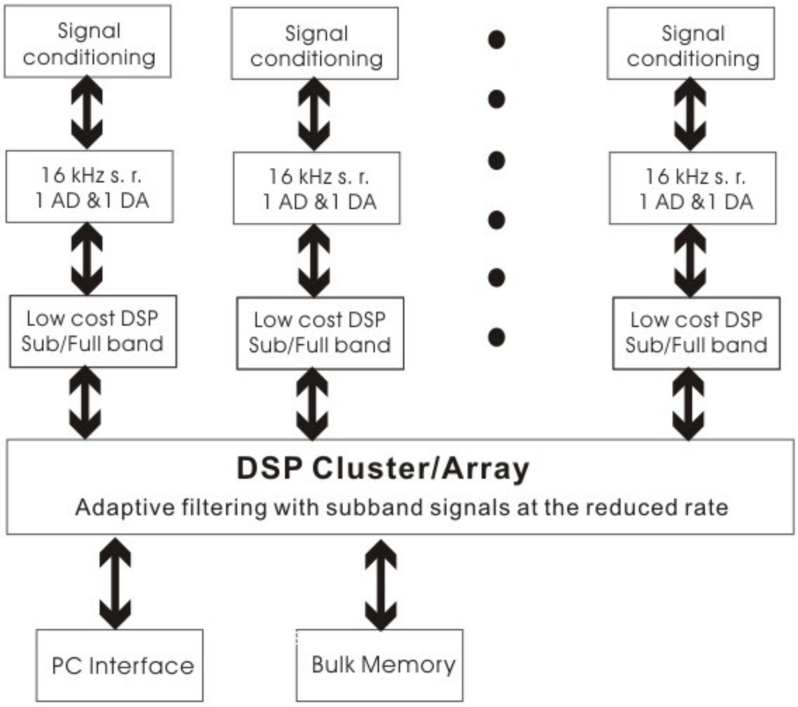

Figure 21. The architecture of the EZ-ANC III.

The main advantages of the EZ-ANC III architecture are:

(1) The flexibility to be expanded to hundreds of channels or to be configured to a specific number of channels as needed. As each front end IO is equipped with a DSP processor, it is able to share the signal processing tasks, and it is possible to add or remove front-end IO channels without changing the hardware of the central processing unit.

(2) The implementation of the multi-rate signal processing techniques allows the IO module to process at a high sampling frequency, which simplifies the signal conditioning hardware, removing the need to add a different anti-aliasing filter or a re-construction filter for each application involving different frequencies to be controlled. It also reduces the computation load of the MFXLMS algorithm significantly and also has the potential to increase the tracking speed of the ANC system

(3) The high sampling frequency and low delay IO module also reduces the delay of the system so that it can result in a higher degree of causality between the reference and error signals and can also be used as a feedback controller.

8. CONCLUSIONS

There are many aspects involved in the development of a successful active noise control system. The team involved in the development must have collective expertise in acoustics, vibration, signal processing, control theory and application, and digital electronic systems. All of this expertise is necessary in order to optimise the performance and stability of an active noise control system. Many of the issues that must be considered in optimising an active noise control system as well as the order in which they should be addressed have been discussed in this paper. Both feedforward and feedback active control systems as well as semi-active systems have been considered, including hardware architectures and software algorithms and some novel ways of improving control system performance have been discussed.

REFERENCES

[1] Hansen, C.H. "Active noise control - from laboratory to industrial implementation", *Proceedings of Noise-Con '97*, Penn State Univ, June 15-17 1997, pp. 3-38.

[2] Hansen, C.H. and Snyder, S.D. *Active control of sound and vibration*. London: E&FN Spon, 1997.

[3] Nelson, P.A. and Elliott, S.J. *Active control of sound*. London: Academic Press, 1992.

[4] Elliott, S.J. *Signal Processing for Active Control*, Academic Press, 2001.

[5] Kuo, S.M. and Morgan, D.R. *Active noise control systems, Algorithms and DSP Implementations*, New York: John Wiley and sons, 1996.

[6] Hansen, C.H., Simpson, M.T. and Cazzolato, B.S. "Genetic algorithms for optimising ASVC systems". **Ch. 9** in *Active sound and vibration control: theory and applications*, pp. 185–220. Number **62** in IEE control engineering series. Institution of Electrical Engineers, London, UK, 2002.

[7] Whitley, D. "The genitor algorithm and selection pressure: Why rank-based allocation of reproductive trials is best", *Proceedings of the Third International Conference on Genetic Algorithms*, George Mason University, Washington DC, 1989, pp.116-121.

[8] Howard, C.Q., Hansen, C.H. and Zander, A.C. "Vibro-acoustic noise control treatments for payload bays of launch vehicles: discrete to fuzzy solutions", *Applied Acoustics*, **66**, 1235-1261 (2005).

[9] Howard, C.Q., Hansen, C.H., and Zander, A.C. "Optimisation of Design and Location of Acoustic and Vibration Absorbers Using a Distributed Computing Network", *Proceedings of Acoustics 2005*, 9-11 November 2005, Busselton, Western Australia, pp.173-178.

[10] Singh, S., Hansen, C.H. and Howard, C.Q. "The elusive cost function for tuning adaptive Helmholtz resonators", *Proceedings of the First Australasian Acoustical Societies' Conference*, November 20-22 2006, Christchurch, New Zealand.

[11] Elliott, S.J., Joseph, P., Bullmore, A.J. and Nelson, P.A. "Active cancellation at a point in a pure tone diffuse sound field." *Journal of Sound and Vibration*, **120**, pp.183-189, (1988)

[12] Elliott, S.J. and David, A. "A virtual microphone arrangement for local active sound control", *Proceedings of the 1st International Conference on Motion and Vibration Control*, Yokohama, 1992, pp.1027-1031.

[13] Roure, A. and Albarrazin, A. "The remote microphone technique for active noise control", *Proceedings of Active '99*, Fort Lauderdale, USA, 1999, pp.1233-1244.

[14] Popovich, S.R. "Active acoustic control in remote regions." US Patent No. 5,701,350, (1997)

[15] Cazzolato, B.S. "An adaptive LMS virtual microphone", *Proceedings of Active '02*, ISVR, Southampton, UK, 2002, pp.105-116.

[16] Haykin, S., *Adaptive Filter Theory*, Prentice Hall, 2002.

[17] Petersen, C.D., Fraanje, R., Cazzolato, B.S., Zander, A.C. and Hansen, C.H. "A Kalman filter approach to virtual sensing for active noise control" submitted to *Mechanical Systems and Signal Processing*, (2006).

[18] Overschee van, P. and Moor de, B. *Subspace Identification for Linear Systems: Theory, Implementation, Applications*. Boston : Kluwer Academic Publishers, 1996.

[19] Petersen, C.D., Zander, A.C., Cazzolato, B.S., Fraanje, R. and Hansen, C.H. "Limits on active noise control performance at virtual error sensors." *Proceedings of Active '06*, Adelaide, South Australia, 2006, pp. 1233-1244.

[20] Zhou, K., Doyle, J.C. and Glover, K. *Robust and Optimal Control*, Prentice-Hall, Inc. New York, 1996.

[21] Petersen, C.D., Zander, A.C., Cazzolato, B.S. and Hansen, C.H. "A moving zone of quiet for narrowband noise in a one-dimensional duct using virtual sensing." *Journal of the Acoustical Society of America*, **121**, (2007).

[22] Petersen, C., Cazzolato, B., Zander, A. and Hansen, C. "Active noise control at a moving location using virtual sensing." Proceedings of the Thirteenth International Congress on Sound and Vibration, Vienna, Austria, 2006.

[23] Petersen, C.D., "Virtual sensing for active noise control at a moving location", Ph.D. Thesis, School of Mechanical Engineering, The University of Adelaide, 5005 SA, Australia, (2007).

[24] Elliott, S.J. and Garcia-Bonito, J., "Active cancellation of pressure and pressure gradient in a diffuse sound field." *Journal of Sound and Vibration*, **186**, 696-704 (1995).

[25] Garcia-Bonito, J., Elliott, S.J. and Boucher, C.C. "A novel secondary source for a local active noise control system." *Proceedings of Active '97*, Budapest, Hungary, 1997, pp. 405-418.

[26] Sommerfeldt, S. "Using energy-based control to achieve global attenuation", *Proceedings of Active '06*, September 18-20, Adelaide, Australia, 2006.

[27] Cazzolato, B.S. and Hansen, C.H. “Active control of sound transmission using structural error sensing”, *Journal of the Acoustical Society of America*, **104**, 2878-2889 (1998).

[28] Cazzolato, B.S. and Hansen, C.H. “Structural radiation mode sensing for active control of sound radiation into enclosed spaces”, *Journal of the Acoustical Society of America*, **106**, 3732-3735 (1999).

[29] Kuo, S.M. and Chen, J. “Multiple-microphone acoustic echo cancellation system with partial adaptive process”, Digital Signal Processing, **3**, (1993).

[30] Kuo, S.M. and Tsai, J. “Acoustical mechanisms and performance of various active duct noise control systems”, *Applied Acoustics*, **41** (1994).

[31] Barrault, G., Halim, D., Hansen, C.H., and Lenzi, A. “An industrial ANC application for an enclosure”, *Proceedings of First Australasian Acoustical Societies' Conference*, Christchurch, New Zealand, November 20-22, 2006 .

[32] Morgan, D.R. and Thi, J.C. “A delayless sub-band adaptive filter architecture”, *IEEE Trans. Signal Processing,* **43**, 1818-1830 (1995).

[33] Huo, J., Nordholm, S. and Zang, Z. “New weight transform schemes for delayless sub-band adaptive filtering”, *Proceedings of IEEE Global Telecommunications Conference*, 2001, pp.197-201.

[34] Larson, L., de Haan, M. and Claesson, I. “A new sub-band weight transform for delayless sub-band adaptive filtering structures”, *IEEE Digital Signal Processing Workshop* 2002, pp.201-206.

[35] Park, S.J., Yun, J.H. and Park, Y.C. “A delayless sub-band active noise control system for wideband noise control”, *IEEE Trans. Speech and Audio Processing*, **9**, 892-899 (2001).

[36] Qiu, X., Ningrong, L., Chen, G. and Hansen, C.H. “The implementation of delayless subband active noise control algorithms”, *Proceedings of Active '06*, September 18-20, Adelaide, Australia, 2006.

[37] Balas, M.J. “Active control of flexible systems”, *Journal of Optimization theory and Applications*, **25** (1978).

[38] Barrault, G., Halim, D., and Hansen, C. “High frequency spatial vibration control using H-infinity method”,. *Journal of Mechanical Systems and Signal Processing* (2006).

[39] Fuller, C.R. and Von Flotow, A.H. “Active control of sound and vibration”, *IEEE Control systems,* December (1995).

[40] de Abreu, G.L.C.M. “Projeto robusto Hinf aplicado no controle de vibrações em estruturas flexiveis com materiais piezoeletricos incorporados”, PhD thesis, Mechanical department of the Federeal University of Uberlândia, Brazil, 2003.

[41] Halim, D. “Vibration analysis and control of smart Structures”, PhD thesis, School of Electrical Engineering and Computer Science, University of Newcastle, Australia, 2002.

[42] Leleu, S. “Amortessiment actif des vibrations d'une structure flexible de type plaque á l'aide de transducteurs piézoelectriques”, PhD Thesis, l'école normale supérieur de Cachan, France, 2002.

[43] Franje, R. “Robust and fast schemes in broadband active noise and vibration control”, PhD. Thesis, University of Twente, Netherlands, 2004.

[44] Haverkamp, B. “State space identification, theory and practice”, PhD. Thesis, Delft University of technology, Netherlands, 2001.

[45] Moheimani, S.O.R., Halim, D. and Fleming, A.J. *Spatial control of vibration: Theory and experiments*, World Scientific Publishing, 2003.

[46] Skogestad, S. and Postlethwaite, I. *Mutlivariable feedback control, Analysis and Design*, John Wiley and Sons, 1996.

[47] Doyle, J.C., Glover, K., Khrgonekar, P.P. and Francis, B.A. “State-space solution to standard H2 and Hinf control problems”, *IEEE Trans. on Automatic Control*, **34** (1989).

[48] Barrault, G. “Controle ativo de vibraçóoes de baixas e altas freqüêencias e ruído radiado de estruturas complexas”, PhD thesis, Federal University of Santa Catarina, Brazil, 2006.

[49] Boudreau. A. and L'Esperance, A. “Accounting for out-of-bandwidth modes in the assumed modes approach: implications on colocated output feeback control”, *ASME Journal of Dynamic Systems, Measurement, and Control*, **119**, 1997.

[50] Barrault, G., Halim, D., Hansen, C. and Lenzi, A. “Optimal truncated model for a flexible structure system within a frequency band”, *Proceedings of Active '06*, Adelaide, Australia, September 18-20, 2006.